ON THE AXISYMMETRIC WAKE OF A DISC IN TURBULENT STREAMS

Elad Rind[1] **and Ian P. Castro**
School of Engineering Sciences
University of Southampton
Southampton, SO17 1BJ, UK
erind@uottawa.ca and i.castro@soton.ac.uk

Introduction

Axisymmetric turbulent wakes have being studied for over half a century, not least because in the far field (when the maximum wake deficit velocity is small in comparison to the free-stream velocity) they are one of the classical free shear flows for which the equations of motion suggest the possibility of self-similar behaviour. In practice many axisymmetric wakes develop in the presence of free-stream turbulence, which for a long time has been known to affect the development of fully-turbulent shear layers. However, in almost all of the published studies on wakes only quiescent streams have been considered, so a thorough investigation of the effects of stream turbulence seems warranted.

For the purposes of the laboratory experiments presented here the free-stream turbulence was generated by bi-planar grids, which provide the classical realisation of (approximately) homogeneous isotropic turbulence (HIT), and the axisymmetric wake generator, a disc, was placed in those streams. Mohamed & Larue (1990), among others, reported that in grid turbulence u'_e/U_0 decays like $z^{-p/2}$ with $p \approx 1.3$, where u'_e and U_0 are the rms and mean velocities, respectively, and z is the axial distance measured from the disc location. Since the high Reynolds number axisymmetric wake's maximum velocity deficit, U_d/U_0, decays like $z^{-2n} = z^{-2/3}$ (Tennekes & Lumley, 1972), one might anticipate that when stream turbulence is added to the wake the parameter u'_e/U_d could remain roughly constant. Note that it can be shown in a similar way that the ratio of the free-stream turbulence axial integral scale to the wake half width L_{ze}/l_h may also be closely constant. However, the current measurements reveal that the mean wake's decay rate is changed by the presence of the free-stream turbulence and that the classical self-similar behaviour ceases to exist. Moreover, it is found that the free-stream turbulence weakens the vortex shedding process in the near wake of the disc and significantly increases the wake's dimensions, yielding an increase in the disc's drag coefficient and thus momentum deficit in the far wake.

Methodology

The University of Southampton's open circuit $3' \times 2'$ wind tunnel was used for this study. The wind tunnel's test section dimensions are 0.6m×0.9m×4.5m and its measured free-stream intensity is below about 0.2%; from now on this will be referred to as the 'uniform' free-stream. The wake's generating body was a 90° conical disc with base diameter of $D = 10$mm. It was mounted in the centre of the test section using a set of Berkley Whiplash Braid Moss Green fishing lines with cross-section diameter of 0.06mm and with its base facing upstream and perpendicular to the flow. (Note that the wire's Reynolds number is about 166 times smaller than the disc's). The disc's Reynolds number based on its diameter, D, and the free-stream velocity, U_0, was about $Re = 15000$ and 5600 for the far and near wake measurements, respectively. Higher turbulence levels (than the wind tunnel's free-stream levels) were generated using two bi-planar grids. One had square aluminium bars and a solidity $d/M \approx 0.27$, where $d = 6.35$mm is the square bar's diameter and M is the mesh spacing; the other had stainless steel rounded bars with $d/M \approx 0.15$, where $d = 1.63$mm.

Measurements in the far wake region were made using a standard constant temperature Hot Wire Anemometry (HWA) system (both AALab AN-1005 and Newcastle NSW bridges were used). The probe used in this work was a standard 45° crossed hot wire with 2.5 μm diameter wires mounted on a Dantec 6mm diameter 55H24 probe support. Each measurement comprised 147 blocks of 16384 samples measured at 10kHz. In addition, two Pitot-static tubes (connected to two Furness Controls limited's FCO12 micromanometers) were used to measure the mean free-stream velocity, one far upstream (used as the wind tunnel reference velocity) and one at the same cross-section as the hot-wire (used to measure the local free-stream velocity during measurements and for reference while calibrating the hot-wire). All analogue signals (both from the hot-wire and the Pitot-static tubes) were digitised using a National Instruments USB-9162 Analog - Digital Converter driven by a suite of linked virtual instruments written in National Instrument's LabVIEW by the EnFlo laboratory at the University of Surrey. In addition to the far wake measurements, near wake flow field measurements were made using LaVision's high frequency 2D Particle Image Velocimetry (PIV) system. This was controlled using LaVision's DaVis Imaging Software, with each measurement comprising 2700 double-frame snapshots taken at 50Hz, with 15μs between each frame of the pair. The snapshots were digital images of

[1]Current address: Department of Mechanical Engineering, University of Ottawa, ON, K1N 6N5, Canada

Grid	Case	Rod shape	$M[mm]$	d/M	$u'_{ze}/U_0[\%]$	L_{11}/D	λ/D	Re_λ
A	1	Square	23.5	0.27	4.3	11	0.21	138
A	2	Square	23.5	0.27	3.7	12.9	0.23	137
A	3	Square	23.5	0.27	3.3	13.7	0.25	134
B	4	Round	11.07	0.15	2.1	3.1	0.15	50
B	5	Round	11.07	0.15	1.2	4.8	0.24	44
B	6	Round	11.07	0.15	0.8	4.8	0.32	43

Table 1. The defining parameters of the different turbulent streams at $z/D = 0$.

1024×1024 pixels, showing an area of about $3.8D \times 3.8D$ at the cross-section through the middle of the disc, captured by the associated fast-frame camera. For more detailed description of the experimental instrumentation and setup see Rind (2011).

Results

First, both the axisymmetric wake behind the disc in the uniform free stream (the 'pure' wake) and the various turbulent free-streams generated by the two grids were studied separately. After some initial development region the pure wake further downstream was found to reach a self-similar state, but this self-similar flow is not a unique one (as shown in the past by, for example, Bevilaqua & Lykoudis, 1978). Thus, the wake decayed according to the expected self-similar power law (see Introduction) while the self-similar profiles showed agreement in trend but not in value when compared to other axisymmetric wakes reported in the literature. The free-stream turbulent flows were also measured and both were found to be similar to previous results for grid turbulence. Once both the wake and turbulent streams were characterised separately, the two grids were each placed at three different locations upstream of the disc, so flows having six different turbulence intensities and length scales at the disc location were available; their characteristics are presented in Table 1. Space restrictions here allow presentation only of results for the wake already embedded in the free-stream turbulence. Measurements of the combined flows were taken downstream of the disc at $z/D = 65, 75, 85, 95, 105$ and 115 for all six cases and are compared to the corresponding pure wake case.

First to be examined here is the axial turbulent stress, $\overline{u_z^2}$. $u'_{z_{max}}$ and $r_{ref} = r\left(u' = u'_{z_{max}}\right)$, where dashed quantities refer to rms values, were used as the wake characteristic velocity and length scales respectively. Figures 1 and 2 show the stress variations for cases one and five, respectively. The results show that the classical self-similar behaviour (where the mean velocity and all the turbulent stress rms values decay at the same rate across the whole wake) no longer exists. In fact the axial turbulence rms, u'_z, decays differently in two distinct regimes across the wake. In the middle part of the wake, u'_z decays at one rate while at the edge of the wake it decays at a rate similar to that of the turbulent stream. Those two regimes are separated by a narrow transition regime which moves inwards with increasing distance downstream. The two decaying regimes were also noticed for the radial and the angular rms quantities, u'_r and u'_θ, respectively (not shown here). Moreover, for these two parameters also, the narrow transition regime moves inwards with distance downstream. Notice in these figures that the data in the central region collapse because they are normalised by a reference within that central region, but this value decays more quickly than the decay of the free stream turbulence so that in the outer region values of

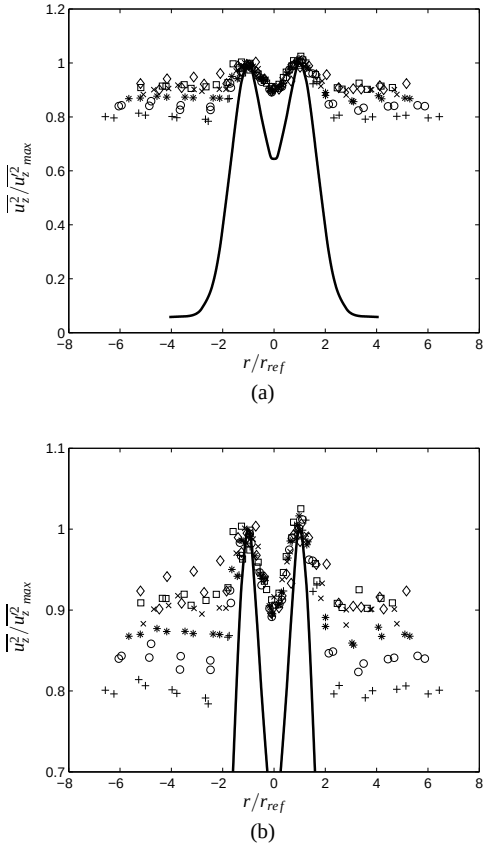

Figure 1. Profiles of the dimensionless normal turbulent velocity fluctuations across the wake for case one. Profiles in (b) are expanded versions of the profiles in (a). Solid lines show the self-similar profile for the pure wake case and $(+)$, $(\circ)$, $(*)$, $(\times)$, $(\square)$ and $(\Diamond)$ refer to $z/D = 65, 75, 85, 95, 105, 115$ respectively.

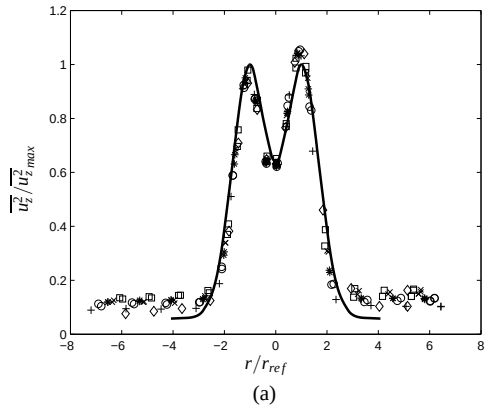

(a)

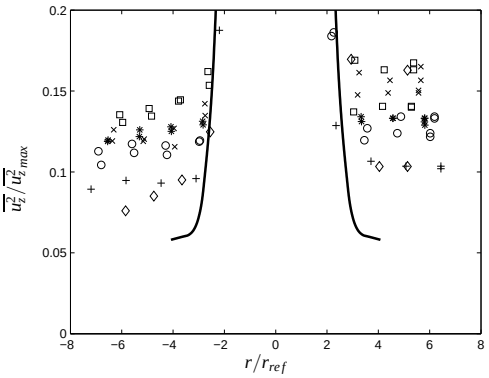

(b)

Figure 2. Profiles of the dimensionless axial velocity fluctuations across the wake for case five. Profiles in (b) are expanded versions of those in (a). Solid lines show the self-similar profile for the pure wake case and $(+)$, $(\circ)$, $(*)$, $(\times)$, $(\Box)$ and $(\Diamond)$ refer to $z/D = 65, 75, 85, 95, 105, 115$ respectively.

$\overline{u_z^2}/\overline{u_z^2}_{max}$ rises with increasing z/D (as clearly seen in figs.1b & 2b). This behaviour occurred in all six cases. Thus, further downstream u'_{ze} must tend towards $u'_{z_{max}}$, although measurements further downstream were not made because there the wake width was no longer small compared with the width of the test section.

Similar data for the other stress components suggest that the turbulence inside the wake becomes increasingly isotropic (based on the simple measure u'_1/u'_2) with an increase in the ratio u'_{ze}/U_0. Thus, the turbulence inside the wake becomes more similar to that in the free-stream. Remember that grid turbulence is very similar to HIT and note as well that measurements for the current grids showed that $u'_1/u'_2 \approx 1.1-1.2$. In addition, it was noticed that the turbulence shear stress peak values are reduced with an increase in the ratio u'_{ze}/U_0, consistent with the wake turbulence becoming more and more like that in the free-stream (HIT) as the ratio u'_{ze}/U_0 increases. Figure 3(a) illustrates a summary of all those findings for all cases. Note however that the shape of the turbulence shear stress profile (where examples for cases one and five are illustrated in figures 3(b) and (c), respectively) suggests that it is still driven by the mean shear and so would only fully cease to

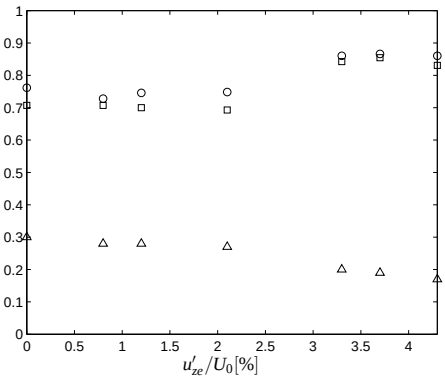

(a)

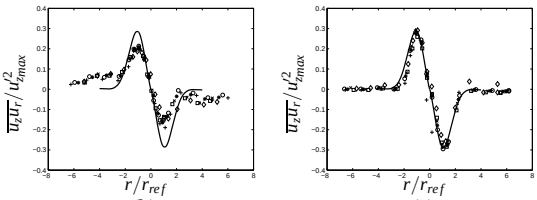

(b) (c)

Figure 3. (a) The ratio between the various turbulence stresses at $z/D = 65$; $\circ$ $u'_{r_{max}}/u'_{z_{max}}$, $\Box$ $u'_{\theta_{max}}/u'_{z_{max}}$ and $\triangle$ $\overline{u_z u_r}_{max}/u'^2_{z_{max}}$. (b) and (c) are profiles of the turbulent shear across the wake for cases one and five, respectively; Solid line is the profile for the pure wake case and $(+)$, $(\circ)$, $(*)$, $(\times)$, $(\Box)$ and $(\Diamond)$ refer to $z/D = 65, 75, 85, 95, 105, 115$ respectively.

exist when the mean shear (or in other words the wake) collapses fully. Thus, the turbulence inside the wake can never be truly similar to that in the free-stream for as long as the wake exists.

The similarity solution for the pure wake has a decay typified by

$$\frac{u'_{z_{max}}}{U_0} = A(z - z_0)^{-2n} \tag{1}$$

where $n = -\frac{1}{3}$. Previous workers have reported different decay rates when the wake is surrounded by stream turbulence, but these studies have had the wake mounted within (or near the exit of) a circular pipe flow, so are less relevant to the present rather 'cleaner' cases. Figure 4 shows the variations of $(u'_{zmax}/U_o)^{-1/2n}$ for the all cases. Note first (in fig.4a for example) that the pure wake data have the expected behaviour, giving a very good fit with a best-fit correlation in excess of 0.999. Secondly, it is clear (from fig.4b) that the grid B data (those with quite low external turbulence levels) also yield reasonably good fits with $n = \frac{1}{3}$ and are also close to the pure wake. Thirdly, however, the Grid A data (fig.4a) do not yield quite such a good fit ($0.989 < R^2 < 0.994$) and lie well below the pure wake data. These wakes have relatively large external turbulence levels and also large ratios of external turbulence integral scale to disc diameter (see Table 1). One should not *a priori* assume that the wakes will decay like the pure wake.

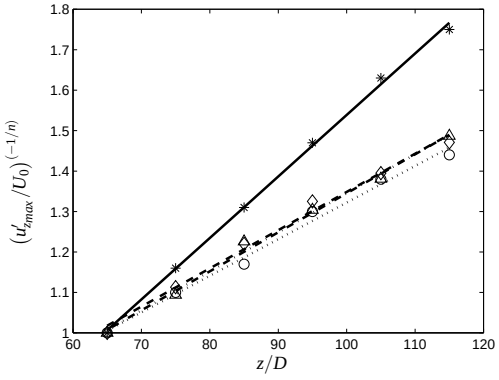

(a)

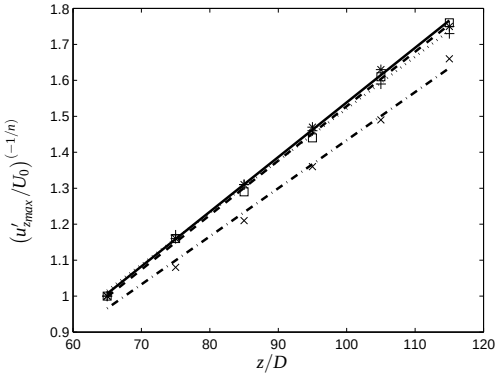

(b)

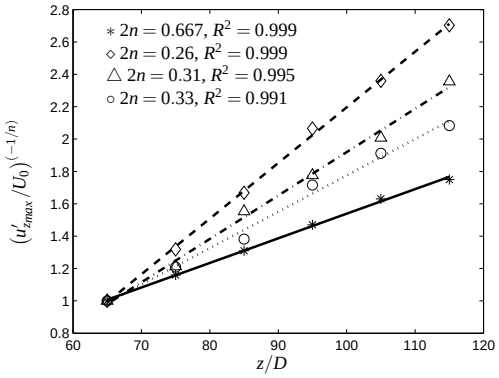

(c)

Figure 4. Variations of $(u'_{z_{max}}/U_0)^{-1/2n}$ with z/D. (a), Cases 1-3 (grid A), with $n = \frac{1}{3}$; case: $\diamond$, 1; $\triangle$, 2; $\circ$, 3. Lines are the corresponding best fits with R^2=: solid line (pure wake), 0.999; dashed line, 0.991, dashed-dot line, 0.994; dotted line 0.989, respectively. (b), Cases 4-6 (grid B), with $n = \frac{1}{3}$; case: $\square$, 4; $\times$, 5; $+$, 6. Solid line, $R^2 = 0.999$; dashed line, 0.991; dashed-dot line, 0.999; dotted line 0.999. (c), as for (a), but values of $2n$ shown in the legend. In all cases, $*$ is the pure wake.

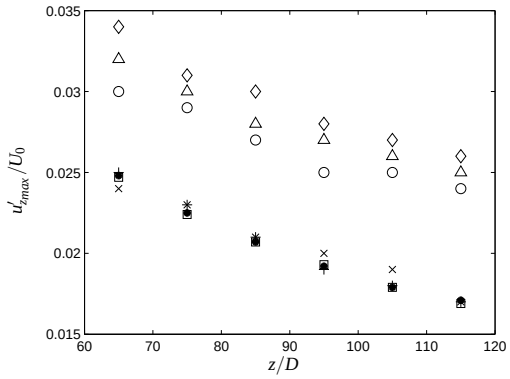

Figure 5. The fall in the maximum wake turbulence level, u'_{zmax} with z/D. Symbols as in fig.4. Note that the grid A data, cases 1-3, have increasing turbulence levels in case order (see Table 1). Note also that grid B data (cases 4-6) collapse with the pure wake data.

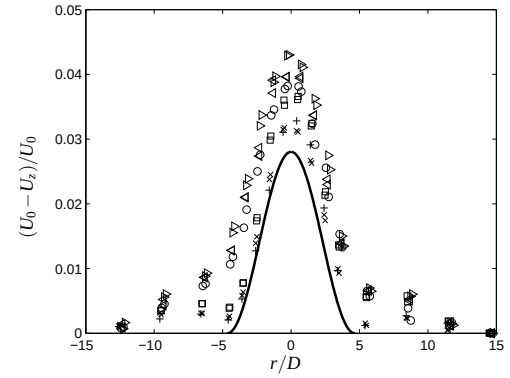

Figure 6. Comparison of the deficit velocity profiles at $z/D = 65$ with the pure wake profile for the six cases; Solid line refers to the pure wake and $(\triangleright)$, $(\triangleleft)$, $(\circ)$, $(\square)$, $(\times)$, $(+)$ are the deficit velocity measurements for cases one, two, three, four, five and six respectively.

Indeed this would seem intuitively unlikely and, in fact, rather better fits can be achieved by reducing the value of n, as shown in fig.4c. Choosing the same $2n$ (0.31) for these three cases would lead to the data all collapsing on a line significantly *above* the pure wake line, but with marginally lower best-fit correlation values. However, caution is necessary here since within the likely experimental uncertainty in u'_{zmax}/U_o a range of n values will achieve reasonable fits to the data in all cases – the z/D range is, after all, relatively small. Nonetheless, the values of u'_{zmax}/U_o at a given x/D are significantly higher in these three (grid A) cases than the pure wake values and they increase with increasing external turbulence level, as shown in figure 5. One could therefore argue that in these cases the external turbulence levels are sufficient to enhance the wake turbulence throughout the whole wake and thus slow down the decay process, leading to a smaller n. The mean velocity data (not shown) also suggested a fall in n for the grid A cases, consistent with the arguments above.

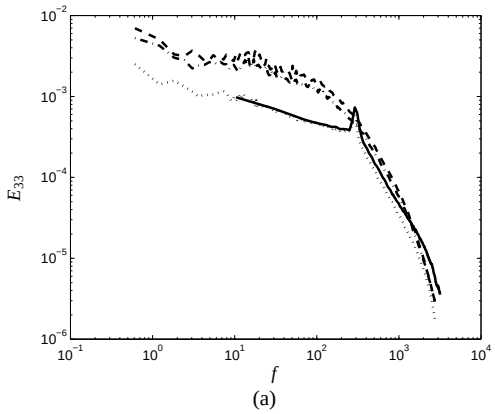

(a)

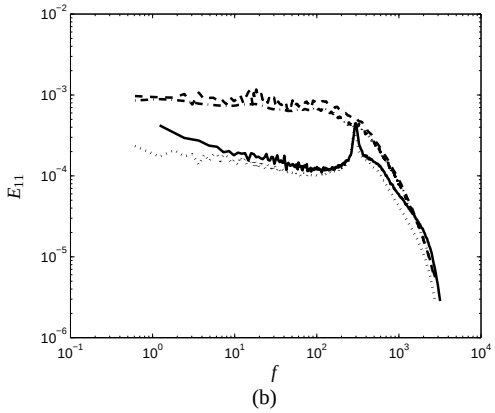

(b)

Figure 7. (a) and (b) are examples of E_{11} and E_{33} vs. f, respectively, at $z/D = 65$ for the pure wake (solid line) and cases 1 (dashed), 3 (dash-dot) & 5 (dotted).

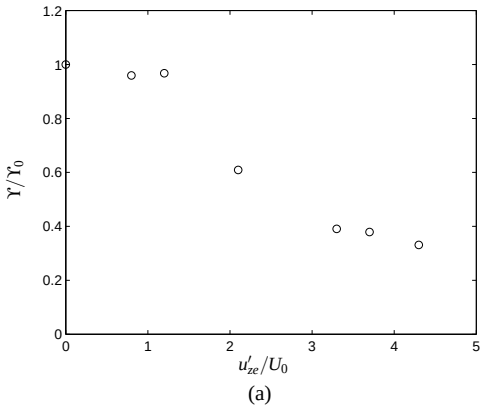

(a)

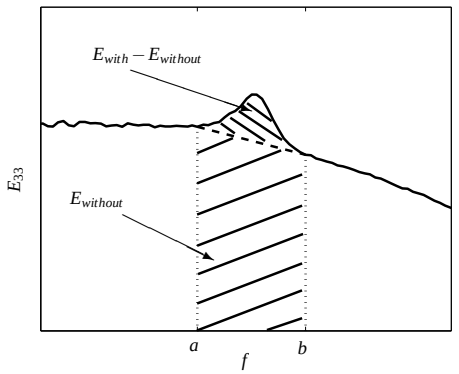

(b)

Figure 8. (a) Variations of the relative energy the shedding process contributes to the E_{33} spectrum with u'_{ze}/U_0 compared with the pure wake case, Υ_0. (b) is an sketch clarifying the definitions of E_{with} and $E_{without}$.

Another clear trend is noticed when mean deficit velocity profiles are compared between the various cases at a specific z/D. The wake centre deficit velocity and its width both increase as u'_{ze}/U_0 increases, as illustrated in figure 6 for $z/D = 65$. This behaviour implies that the disc's drag coefficient is increased due to the presence of the free-stream turbulence. This is consistent with the near-wake PIV measurements (not shown), which revealed that the recirculation length decreased with increasing u'_{ze}/U_0, no doubt due to the increased entrainment into the separated shear layer. Recall that it has been found by both Bearman (1965) and Bearman & Trueman (1972) that the nearer to the body the vortices form the lower is the base pressure (and thus the higher the drag).

Finally, we consider the energy spectrum (measured in the far-wake regime). Figures 7(a) and (b) show examples of the axial and radial spectrum (E_{33} and E_{11} respectively) around the wake half width at $z/D = 65$ for the pure wake and cases 1, 3 & 5. Note first that the rms value of the radial velocity (related to the area under the plots in fig.7b) is increased by a factor of about three – much higher than the increases in the axial rms (seen in fig.5 and implied by fig.7a). Secondly, it is clear that in grid A cases (1-3) the vortex shedding frequency is no longer noticeable in the spectra of the axial and radial velocities, whereas it remains visible in case B cases (4-6). In the pure-wake case the vortex shedding frequency is easily noticeable in both the axial and radial energy spectra. Thus, since the free-stream turbulence levels at $z/D = 0$ varied roughly monotonically at $z/D = 0$ with cases 1-6 (see table 1) and there seems no continuously monotonic variation in the wake behaviour across all six cases, it could be argued that the significant differences between grid A and grid B cases is a result of the very different levels of L_{11}/D at $z/D = 0$ for the two grids. The most significant effects occur when L_{11}/D is O(10), rather than much smaller, presumably leading to significant large-scale 'shaking' of the wake in its very early stages. On the other hand, in the far-wake region the ratio $u'_{ze}/u'_{z_{max}}$ is much larger in grid A than in grid B cases so it could be argued that it is this parameter in the far wake region which causes the difference.

In order to understand better the disappearance of the vortex shedding signal, near-wake flow field measurements (using PIV) and spectral measurements (at a fixed location, about $4-5D$ downstream of the disc) were made. Note that the near-wake flow field and spectral measurements were made at $Re = 6500$, due to hot-wire mounting and PIV limitations at high speeds in the near-wake region. Note also that the dimensionless vortex shedding frequency ($St = f_s D/U_0$, where f_s is the shedding frequency) was found to be Reynolds

number independent in the $5000 < Re < 15000$ regime.

The spectral data showed that the vortex-shedding frequency rises by less than 10% as the external turbulen levels rise (from cases 1-6). Similar rises were noticed by Castro (1995) for wakes downstream of a ring. He suggested that the increase in the rate at which vortices are shed is associated with a reduction in the length of the recirculating region (which, as mentioned above, does indeed become shorter with increasing u'_{ze}/U_0). On the other hand, despite this small rise in shedding frequency, figure 8(a) shows that the addition of stream turbulence strongly weakens the relative energy the shedding process contributes to the spectrum. We define Υ by $\Upsilon = (E_{with} - E_{without})/E_{without}$, where $E = \int_a^b E_{33}\mathrm{d}f$, $[a,b]$ is the range of frequencies bounding the vortex shedding peak and the subscripts *with* and *without* specify, respectively, whether the peak is included or excluded from the integral. This is a measure of the relative vortex shedding strength. Figure 8(b) is a sketch clarifying this definition. Fig.8(a) shows that Υ falls by around 70% as the external turbulence levels increase. This significant weakening of the vortex-shedding process has been noticed before in the context of several different objects in turbulent streams, e.g. Gerrard (1966) and Tyagi, Liu, Ting & Johnston (2005). Thus, the fact that the vortex-shedding energy is reduced (at the creation process) combined with the fact that it is being continuously reduced with distance downstream, explains why it becomes harder to trace, or even (for case A cases) is absent entirely in the far-wake spectral measurements.

In addition, since in the near wake regime the turbulence levels inside the wake were noticed in the PIV measurements to be gradually increasing with u'_{ze}/U_0 whilst the vortex-shedding strength is reduced due to the increased entrainment in the separated shear layer (see Gerrard, 1966), the relative contribution to the spectrum would necessarily be reduced. Thus, there would be a point (at high enough u'_{ze}/U_0) where the spectral peak would not be easily traceable even in the near-wake regime, as Mujumdar & Douglas (1970) noticed two diameters downstream of a sphere in turbulent streams.

Conclusions

Wind-tunnel experiments were undertaken in order to study the influence free-stream turbulence has on axisymmetric wakes. It was found that the free-stream turbulence affects the wake's mean and turbulence structure and their development. It was also found that the level at which the free-stream turbulence affects the far wake is related to the ratio between the turbulence levels inside and outside the wake and perhaps also by the ratio of external turbulence length scale and the wake width in the near-wake region. In addition, it has been shown that the classical self-similar solution is no longer valid when external turbulence exists; the latter gradually penetrates the wake resulting, if it is strong enough, in a different wake decay rate which seems to be much slower than that of the pure wake. This is contrary to the findings of Legendre, Merle & Magnaudet (2006); Wu & Faeth (1994), who found more rapid decays, but this was in the context of different kinds of external turbulence (and also with external mean velocity shear). The effects identified here are associated not only with conditions in the far-wake region but also during the wake's creation. Thus, the initiation of the wake clearly controls some of its specifying properties far downstream. We mention finally that the work was done simultaneously with extensive direct numerical simulations of equivalent time-developing flows. That work is being published separately (Rind & Castro, 2011).

Acknowledgments

We would like to acknowledge the School of Engineering Sciences at the University of Southampton for funding E. R. via a research scholarship. In addition, we would like to express our great gratitude to Dr Gary N. Coleman, Dr. Victoria Suponitsky, Dr Paul Hayden and Mr Zachary Taylor for their input throughout our long discussions.

REFERENCES

BEARMAN, P. W. 1965 Investigation of the flow behind a two-dimentional model with a blunt trailing edge and fitted with splitter plates. *J. Fluid Mech.* **21**, 241–255.

BEARMAN, P. W. & TRUEMAN, D. M. 1972 An investigation of the flow around rectangular cylinders. *Aeronautical Quarterly* **23**, 229–237.

BEVILAQUA, P. M. & LYKOUDIS, P. S. 1978 Turbulence memory in self preserving wakes. *J. Fluid Mech.* **89**, 589–606.

CASTRO, I. P. 1995 Vortex shedding from a ring in turbulent flow. *European Journal of Mechanics. B, Fluids* **14** (3), 245–262.

GERRARD, J. H. 1966 The mechanics of the formation region of vortices behind bluff bodies. *J. Fluid Mech.* **25**, 401–413.

LEGENDRE, D., MERLE, A. & MAGNAUDET, J. 2006 Wake of a spherical bubble or a solid sphere set in fixed in a turbulent environment. *Phys. Fluids A* **18**, 048102–1–4.

MOHAMED, M. S. & LARUE, J. C. 1990 The decay power law in grid generated turbulence. *J. Fluid Mech.* **219**, 195–214.

MUJUMDAR, A. S. & DOUGLAS, W. J. W. 1970 Eddy shedding from a sphere in turbulent free-streams. *Int. J. Heat Mass Transfer* **13**, 1627–1629.

RIND, E. 2011 Turbulent wakes in turbulent streams. PhD Thesis, University of Southampton, UK.

RIND, E. & CASTRO, IAN P. 2011 Direct numerical simulation of axisymmetric wakes embedded in turbulence (To be submitted). *J. Fluid Mech* .

TENNEKES, H. & LUMLEY, J. L. 1972 *A First Course in Turbulence*. The MIT Press.

TYAGI, H., LIU, R., TING, D. S.-K. & JOHNSTON, C. R. 2005 Experimental study of vortex shedding from a solid sphere in turbulent freestream. *Proceedings of 2005 ASME Fluids Engineering Division Summer Meeting, FEDSM2005* **V2005**, 561–569.

WU, J.S. & FAETH, G.M. 1994 Effect of ambient turbulent intensity on sphere wakes at intermediate reynolds numbers. *AIAA J.* **32**, 535ff.